AIAA SciTech Forum
7-11 January 2019, San Diego, California
AIAA Scitech 2019 Forum

10.2514/6.2019-1340



# Geometry Effects on the Galloping Instability of Rectangular Cylinders at Low Reynolds Number

Mark A. Feero*, Ahmed M. Naguib†
and Manoochehr M. Koochesfahani‡
*Michigan State University, East Lansing, Michigan, 48824, USA*

**Wind tunnel experiments were used to investigate the effects of geometry on the transverse galloping behavior of nominally rectangular cylinders at Reynolds numbers from 1000 to 10,000. Static measurements of the lift and the drag forces were used to determine the variation of the normal force coefficient with angle-of-attack, in accordance with the typical quasi-steady description of galloping. Cylinders with unity chord-to-thickness ratio (side ratio) were found to vary from unstable, to neutrally stable, to stable as the corner radius was increased from sharp, to half-round, to fully-round. Cylinders with side ratios of 2 or 3 demonstrated either stability over the entire Reynolds number range, or a transition from unstable to stable with increasing Reynolds number, depending on corner radius. The results demonstrated that in general, increasing the corner radius had a stabilizing effect.**



## I. Introduction

Elastically mounted cylinders with non-circular cross section are susceptible to a flow induced instability known as galloping due to the fact that the aerodynamic forces on the body change with its orientation to the oncoming flow. When a cylinder is elastically mounted in the transverse direction, i.e. the $y$-direction as defined in Figure 1, an oscillation velocity $\dot{y}$ in this direction will cause a change in the cylinder's effective angle-of-attack, $\alpha$. As such, oscillating lift and drag forces will occur. The normal force coefficient along the $y$-direction is related to the lift and drag coefficients, *viz.*:

$$C_y = \frac{F_y}{1/2\rho U_\infty^2 dl} = -\frac{1}{\cos\alpha^2}(C_L\cos\alpha + C_D\sin\alpha), \tag{1}$$

where $C_L = F_L/(1/2\rho U_{\text{rel}}^2 dl)$ and $C_D = F_D/(1/2\rho U_{\text{rel}}^2 dl)$ are the lift and the drag coefficients, respectively, $U_\infty$ is the steady freestream velocity, $U_{\text{rel}}$ is the instantaneous oncoming velocity relative to the cylinder, $\rho$ is the fluid density, $d$ is the cylinder width and $l$ is the cylinder span. $F_L$ and $F_D$ are the lift and the drag forces, respectively, and $F_y$ is the normal force. If the oscillation in $F_y$ is such that it increases with $\alpha$, this effectively produces negative fluid damping and the structure could become unstable; a phenomenon known as transverse galloping. That is, if $\partial C_y/\partial\alpha > 0$, the cylinder meets the necessary aerodynamic condition for galloping. Galloping is a phenomenon that can affect structures such as ice coated power lines, bridge decks and stalled wings [1]. Another type of structure that may be susceptible to the galloping instability is the suspension line used in parachutes [2], such as those used to attach the payload to the canopy in precision airdrop systems [3]. The cross-section of these braided cables is not circular, but is more accurately described as a rectangle with a side ratio $c/d$ (where $c$ is chord length) in the range $2-3$ and rounded corners [2]. Understanding the aerodynamic behavior relating to the transverse galloping of such nominally rectangular cylinders is therefore fundamental to the prediction and mitigation of this instability.

The analysis of galloping typically assumes that the forces acting on the body vary in a quasi-steady manner; that is, the lift and the drag forces depend only on the instantaneous relative velocity, $U_{\text{rel}}$. However,

*Postdoctoral research associate, Department of Mechanical Engineering, Michigan State University Michigan, USA, AIAA Member
†Professor, Department of Mechanical Engineering, Michigan State University Michigan, USA, AIAA Associate Fellow
‡Professor, Department of Mechanical Engineering, Michigan State University Michigan, USA, AIAA Associate Fellow

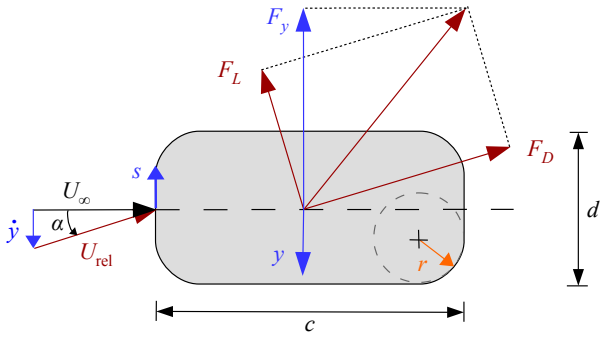


Figure 1: Rectangular cylinder cross-section geometry and forces acting on the body when moving in the transverse direction at a velocity $\dot{y}$.



this assumption is only valid when the time scale of oscillation is much longer than the time scale associated with vortex shedding in the wake of the body. The relevant time scale ratio is expressed non-dimensionally as the reduced velocity $\mathrm{Vr} = U_\infty/(df)$, where $f$ is the frequency of oscillation. Classically, it has been argued that quasi-steady analysis is valid for $\mathrm{Vr} > 20$ [1]. Bearman and Luo [4] showed that the validity of the quasi-steady assumption is better correlated to both the reduced velocity and the amplitude of oscillation. If the assumption of quasi-steady behavior can be considered valid, then the results from static wind tunnel tests can be used to describe the variation of the aerodynamic forces with $\alpha$.

The goal of the present study is to investigate the effects of geometry on the aerodynamic behavior of nominally rectangular cylinders with side ratio $c/d$ and corner radius ratio $r/d$ as it pertains to the transverse galloping instability. This is a fundamental investigation in the behavior of rectangular cylinders that are relavent to the application of parachute suspension lines. This work is motivated by recent experimental studies from Siefers *et al.* [2, 5] who showed that large amplitude oscillations were present on suspension lines at frequencies much lower than those of vortex shedding in the wake, and the authors suspected transverse galloping could be the cause. The Reynolds number range considered in this work is $Re_d = U_\infty d/\nu = 1000$ – 10,000, where $\nu$ is the kinematic viscosity, which is relevant to the suspension lines of precision airdrop systems. Over this relatively low Reynolds number range, there is limited information in the literature on the flow characteristics of rectangular cylinders, even for sharp-cornered cylinders. To the best of the authors knowledge, there have been no studies regarding the effect of corner radius on galloping for $c/d > 1$. In this work, static wind tunnel testing on geometries with $1 \leq c/d \leq 3$ and $0 \leq r/d \leq 0.5$ was performed to determine the variation in the lift and the drag forces, and surface-pressure distributions with angle-of-attack on rigidly mounted models. The $\alpha$ variation in $C_y$ was computed from $C_L$ and $C_D$, and from this the $\partial C_y/\partial\alpha$ galloping criterion was assessed.

## II. Experimental Setup

The experiments are conducted in a low-speed, low-turbulence open return wind tunnel located at the Flow Physics and Control Lab at Michigan State University. Flow enters the test section after passing through a series of screens, a honeycomb and a 10:1 contraction. The test section has a 355 mm × 355 mm square cross-section and is 3 m long. The mean turbulence intensity at the center of the test section over the range of freestream speeds used in this study is 0.1% for a frequency range above 0.5 Hz. The Reynolds number varies from $Re_d = 1100$ to 10,000, which corresponds to freestream velocities of approximately 0.8 m/s to 7.5 m/s. The freestream velocity is monitored using a pitot-static tube connected to an MKS Baratron 223B differential pressure transducer with a full-scale range of 133 Pa and a 0.3% of-reading accuracy. At the low Reynolds number end, the pressure transducer resolution becomes a greater source of uncertainty than the accuracy, with a resolution of 0.013 Pa.

The experimental models under investigation are cylinders with nominally rectangular cross-section defined by the chord length $c$, the diameter $d = 20$ mm, and the corner radius $r$, as shown in Figure 1. The coordinate $s$ is the in-plane surface tangential direction, originating at the forward intersection of the chord

line and the model surface. The cross-sectional shapes of the nine models are shown in Figure 2. The case of $r/d = 0.5$ corresponds to cylinders with fully round fore and aft faces, while $r/d = 0$ is the sharp-edged case. The models are 320 mm in length and span the majority of the test-section height, giving an aspect ratio of 16. The nominal solid blockage at an angle-of-attack $\alpha = 0°$ is 5%, and the worst case blockage for $c/d = 3$ and $\alpha = 15°$ is 10%. Circular end plates with a diameter of $15d$ and a 30° chamfered edge are fixed to the walls of the tunnel at each end of the model (Figure 3a). In order to allow free movement of the model under aerodynamic loading for force measurements, a 30 mm long by 20 mm wide slot is necessary in the end plates. Initial testing showed that outside air drawn into the test-section through this slot had significant impact on the flow. As such, $4.5d$ diameter, 0.75 mm thick fences are attached to the ends of the model to eliminate the unwanted axial flow. A gap of approximately 0.5 mm is maintained between the fences and the fixed end plates, as shown in Figure 3a.

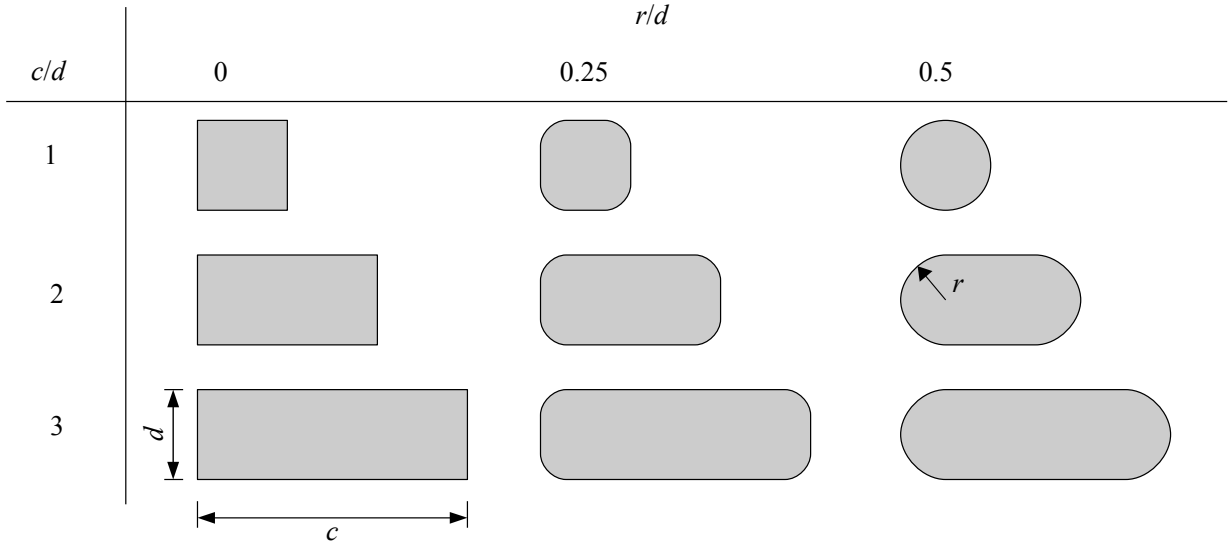


Figure 2: Cross-sectional geometry of the models under investigation.

The models are constructed using one of two methods. For geometries where only force measurements are performed, the model is machined from a single piece of aluminum. When surface pressure measurements are desired, the model is made in three spanwise segments; two outer aluminum segments, and a center 3D printed segment housing the pressure taps. Pressure taps with a diameter of 0.35 mm are distributed around the perimeter of the model with a typical spacing in the $s$-direction of $0.02P$, where $P$ is the model perimeter. Where necessary, the spanwise location of successive taps is staggered to accommodate the connection of plastic tubing inside the model. For the $c/d = 1$ models, only half the perimeter houses pressure taps due to limited space for tubing inside the model. In this case, full pressure distributions are measured by first measuring at $\alpha$, and then $\alpha + 180°$. A step-servo motor with a resolution of 0.02° is used to control $\alpha$. The tubing is connected to a 48 channel Scanivalve and the pressure is measured using an MKS Baratron 226A transducer with 133 Pa range. This sensor has a 0.3% of-reading accuracy and a resolution of 0.013 Pa.

A custom one-component force balance is used to measure the lift and the drag forces on the model. Given the Reynolds number range of interest, these forces are very low in magnitude. For example, at $Re_d = 1000$ a drag coefficient $C_D = 1$ corresponds to a force of approximately 2.5 mN given the model dimensions. The force balance, shown in Figure 3b, is comprised of a parallelogram four bar linkage from which the model is suspended. Given the length of the bars from which the moving plate is suspended, the balance moves primarily unidirectionally as the vertical displacement is $\mathcal{O}(10^2)$ – $\mathcal{O}(10^4)$ times smaller than the horizontal. The angular motion at the pivot points is accomplished using Riverhawk 6016-600 rotational flexures that have no surface-on-surface contact, thus avoiding static-friction issues. The loads that oppose the motion of the balance and provide the necessary stiffness are the total suspended weight and the torque at the pivot points. By measuring the displacement of the balance in the force direction using a Baumer OADM 12U6430 non-contact triangulation laser displacement sensor ($3 - 5$ $\mu$m resolution), the force can be obtained

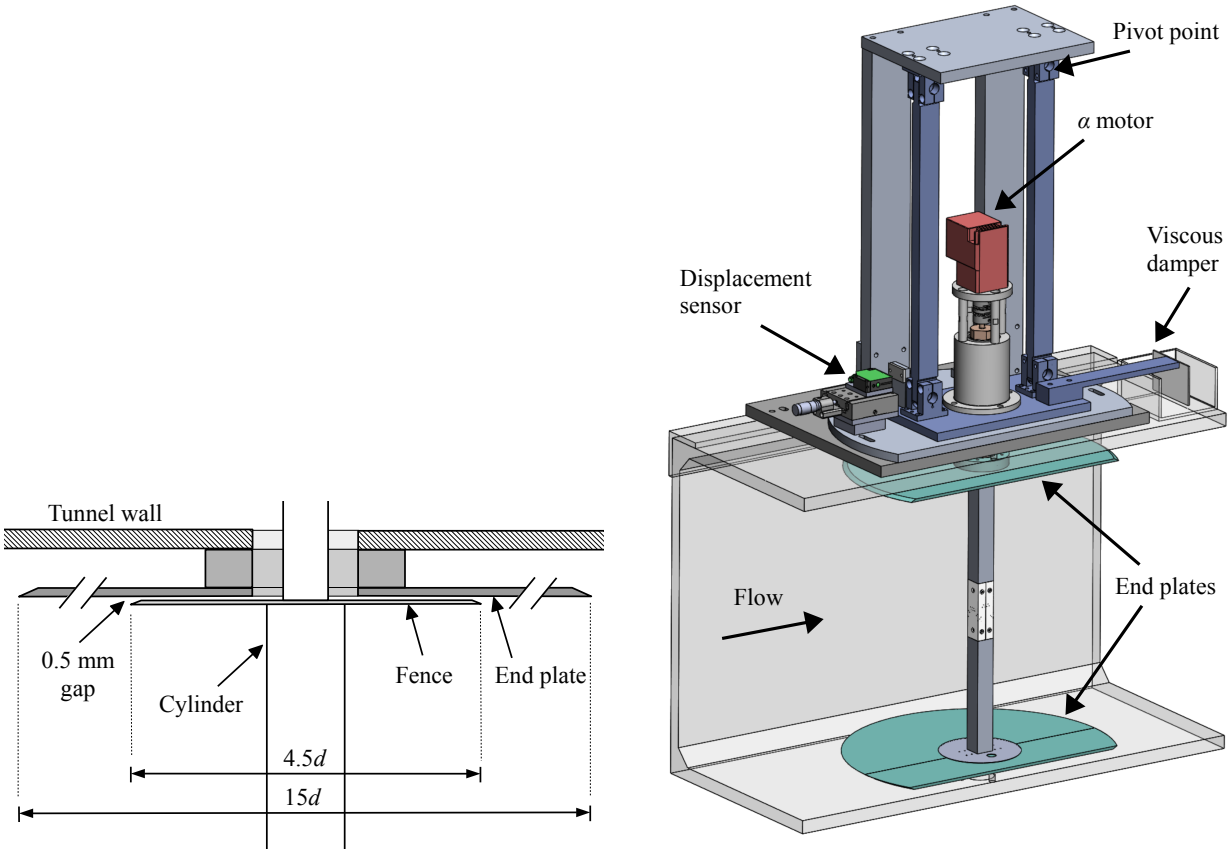


(a) End conditions at the upper end of the model showing the fixed end plate and the moving fence.

(b) Cut-away view of the complete experimental setup including the force balance, rotation assembly, model and end plates.

Figure 3: Experimental setup schematics.



if the stiffness is known. An *in-situ* calibration is performed by applying known loads and measuring the displacement. The balance is calibrated over a range of 2.5 mN – 500 mN and a typical stiffness is $110 \pm 1$ N/m. Extensive calibrations have shown that the response of the balance is linear over the entire calibrated range. The full balance assembly is mounted to a platform that can be rotated to change between lift and drag measurement; the configuration in Figure 3b shows the balance in the drag measurement position. A viscous damper, composed of a mesh plate in an oil reservoir, is necessary to damp the oscillations of the balance at its natural frequency of 1 Hz. For a $c/d = 1$, $r/d = 0$ cylinder with a non-dimensional vortex shedding frequency of 0.13 [6], the expected shedding frequency is 4 Hz at $Re_d = 1000$. These oscillations have negligible effect on the mean forces as they are also very low in amplitude due to the damping, with a maximum amplitude of approximately $0.01d$ at the highest Reynolds number. The repeatability in the force measurements varies from 0.1 mN – 1 mN over $Re_d = 1100 - 10{,}000$. Prior to use in the present experiments, the force balance was validated using measurements of drag on a circular cylinder. This validation along with other aspects of the force balance accuracy are the subject of a separate manuscript.

## III. Results

### A. Sharp-cornered square cylinder

Examples of the directly measured $C_L$ and $C_D$ variation with $\alpha$ are shown in Figure 4 for the $c/d = 1$, $r/d = 0$ model. Five different Reynolds numbers are considered: $Re_d = 1100$, 2500, 5000, 7500 and 10,000. The ranges of measurement uncertainties in $C_D$ and $C_L$ are 0.02 – 0.07 and 0.002 – 0.06, respectively. For

$Re_d > 1100$, the variation in $C_D$ with $\alpha$ is approximately parabolic at low $\alpha$, with a local maximum occurring at $\alpha = 0°$. This behavior of a maxima in drag at $\alpha = 0°$ was not consistent over the entire geometry range; although not shown for brevity, some of the models with larger $c/d$ displayed the inverse trend of a local minimum in drag at $\alpha = 0°$. At $Re_d = 1100$, there is a substantial decrease in $C_D$ and a flattening of the curve for $-5° \leq \alpha \leq 5°$. Beyond this flat section, $C_D$ continues to decrease with $\alpha$ up to 15°, which is similar to the behavior at $Re_d = 2500$. For $Re_d \geq 5000$, there is a drastic change in $C_D$ at $\alpha = 12°$ where the slope of the curve sharply reverses and drag begins to increase. This change with Reynolds number is also reflected in the lift coefficient, where $C_L$ monotonically decreases with $\alpha$ for $Re_d < 5000$, but a reversal in the $C_L$ slope occurs at $\alpha = 12°$ for $Re_d \geq 5000$. The drastic change in $C_D$ and $C_L$ at $\alpha = 12°$ is due to flow reattachment on the bottom face, which is a well known effect for square cylinders with $r/d = 0$ (e.g. [7]), and the angle where reattachment occurs is often referred to as the critical angle. This value of the critical angle and it's insensitivity to Reynolds number agree very well with other studies who all found reattachment to occur at $\alpha = 12°$ for $5000 \leq Re_d \leq 37,000$ [8, 9, 10]. The presence of a negative $C_L$ slope at each Reynolds number indicates the possibility of galloping, since it can be shown that $\partial C_y/\partial\alpha > 0$ is equivalent to $\partial C_L/\partial\alpha + C_D < 0$ for small $\alpha$ [1].

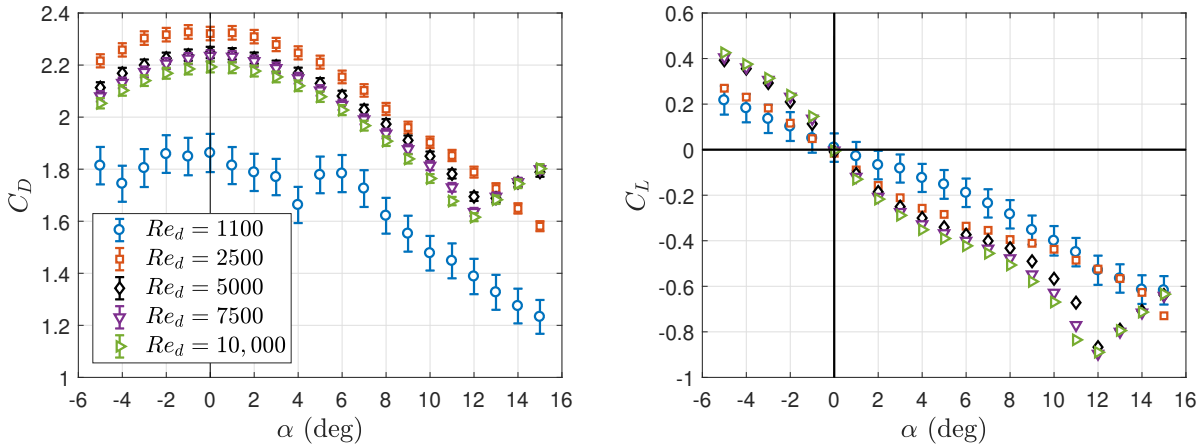


Figure 4: Drag and lift coefficients for the $c/d = 1$, $r/d = 0$ cylinder as a function of angle-of-attack and Reynolds number. Other than $Re_d = 1100$, the errorbars on $C_L$ are less than the marker size.

Prior to considering the results for the other geometries, the galloping behavior of the $c/d = 1$, $r/d = 0$ case will first be discussed since there exists data regarding this geometry from previous studies. Figure 5a shows the variation in the normal force with $\alpha$ computed using $C_D$ and $C_L$ from Figure 4. As discussed in Section I, the sign of $\partial C_y/\partial\alpha$ indicates stability with respect to transverse galloping. In particular, a shape is often deemed "unstable" with respect to galloping when $\partial C_y/\partial\alpha > 0$ at $\alpha = 0°$, since this corresponds to a body galloping from rest. If $\partial C_y/\partial\alpha < 0$ at $\alpha = 0°$, but the slope in $C_y$ is positive at some $\alpha$ range away from 0°, the body can still gallop as a hard oscillator. Hard galloping will be discussed in a subsequent section. The results in Figure 5a demonstrate that for $Re_d > 1100$, $\partial C_y/\partial\alpha > 0$ at $\alpha = 0°$ and the body is unstable. At $Re_d = 1100$, the change in $C_y$ near $\alpha = 0°$ is negligible within the error bounds, thus the body is neutrally stable at this Reynolds number. The severity of the galloping instability can be quantified by examining the magnitude of $\partial C_y/\partial y$, which is shown in Figure 5b for $\alpha = 0°$. The derivative was computed from either a cubic spline fit of $C_y$, or a sliding cubic fit for $Re_d < 5000$ to smooth scatter in the data. Over $1100 \leq Re_d \leq 10,000$, the derivative of $C_y$ increases monotonically from a value that is zero (within uncertainty) to $6.4 \pm 1.2$. This indicates that the cylinder becomes more susceptible to galloping with increasing Reynolds number. Data from previous studies up to $Re_d = 66,000$ is also included in this figure for comparison with the present results. The only value of $\partial C_y/\partial\alpha$ that overlaps the present Reynolds number range is from Norberg [10] at $Re_d = 5000$, which agrees within uncertainty with the present value of $\partial C_y/\partial\alpha$ at the same $Re_d$. The combination of the data from this study and that of other researchers shows a maximum in $\partial C_y/\partial y \approx 6$ at $Re_d \approx 10,000$, with the value at higher Reynolds number potentially plateauing at $Re_d \approx 30,000$ at a value of $\partial C_y/\partial y = 2 - 3$. It is often assumed that the effect of Reynolds number on

the galloping behavior of rectangular cylinders with $r/d = 0$ is negligible due to their fixed separation points (e.g. [11]). However, the present results and those of other studies demonstrate that quite the opposite is be true for $c/d = 1$.

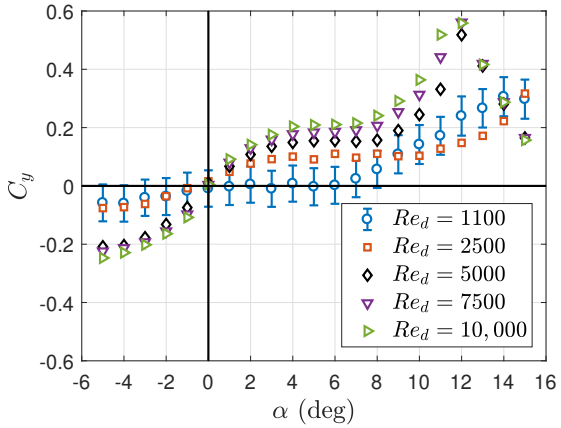


(a) Normal force coefficient variation with $\alpha$ and $Re_d$. Symbols are the same as in Figure 4 and errorbars are less than the marker size for $Re_d > 1100$.

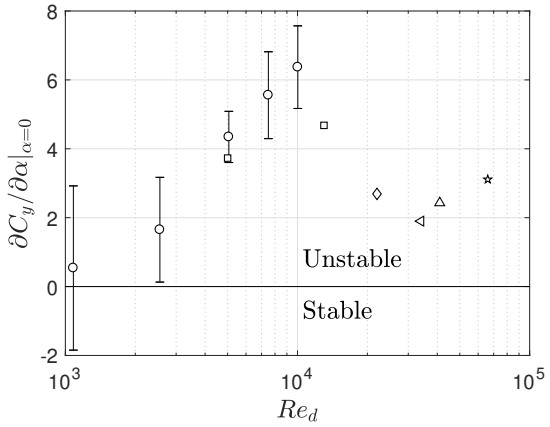


(b) Dependence of the normal force coefficient derivative at $\alpha = 0°$ on $Re_d$. (○) Present, (□) Norberg (1993) [10], (◇) Parkinson & Smith (1964) [12], (◁) Luo *et al.* (1994) [9], (△) Piccardo *et al.* (2011) [11], (⋆) Parkinson & Brooks (1961) [13].

Figure 5: Galloping stability for $c/d = 1$, $r/d = 0$.

## B. Normal force coefficients and galloping behavior

The $C_y$ variation with $\alpha$ and $Re_d$ for each of the geometries shown in Figure 2 is shown in Figures 6, 7 and 8 for $c/d = 1$, 2 and 3, respectively. The $c/d = 1$, $r/d = 0.5$ case is not shown since this geometry is stable be definition. The results are grouped by $c/d$ since the maximum value of $C_y$ increases substantially with increasing $c/d$ for each $r/d$.

The results for $c/d = 1$, shown in Figure 6, will first be considered. The previously shown plot of $C_y$ for $c/d = 1$, $r/d = 0$ is reproduced in this figure for direct comparison with $r/d = 0.25$. After the region of positive $\partial C_y/\partial\alpha$ for $r/d = 0$ and $Re_d > 2500$, the slope becomes flat for $\alpha \approx 4°$ to 7°, prior to increasing once again up to the critical angle of 12°. Beyond this angle, the slope in $C_y$ becomes negative and the body is stable. $Re_d = 2500$ displays a similar trend, however there is no reattachment at this Reynolds number and $\partial C_y/\partial\alpha$ remains positive after $\alpha = 10°$. Comparing $C_y$ for $r/d = 0.25$ to $r/d = 0$, a drastic change is observed. At this increased value of $r/d$, the slope in $C_y$ near $\alpha = 0°$ is zero for $Re_d > 1100$, indicating the body is neutrally stable. A slight positive slope is observed for $Re_d = 1100$, although given the error bounds on $C_y$, the slope may still be very near zero. For $2500 \leq Re_d \leq 7500$, an $\alpha$ range away from zero is observed where $\partial C_y/\partial\alpha$ becomes positive, and this range both shrinks in size and becomes farther from $\alpha = 0°$ with increasing Reynolds number. After this range of positive $\partial C_y/\partial\alpha$, $C_y$ begins to decrease and the body is stable. Once $Re_d = 10,000$ is reached, $C_y$ is essentially flat up to $\alpha = 11°$, after which $\partial C_y/\partial\alpha < 0$. These results demonstrate that for $c/d = 1$, the corner radius has a profound effect on galloping behavior and the resistance of a cylinder with unity side ratio to galloping can be improved by increasing $r/d$.

The variation in $C_y$ with $\alpha$ for $c/d = 2$ is shown in Figure 7 for $r/d = 0$, 0.25 and 0.5. For $r/d = 0$, the results are reminiscent of those for $c/d = 1$ at the same $r/d$, although at this larger side ratio $\partial C_y/\partial\alpha$ is positive at $\alpha = 0°$ for the entire Reynolds number range. The $C_y$ curves also show a sharp change from $\partial C_y/\partial\alpha > 0$ to $\partial C_y/\partial\alpha < 0$ at a lower angle-of-attack than for $c/d = 1$. This angle decreases from approximately 8° to 6° with increasing $Re_d$, and it is possible that this represents similar flow reattachment behavior as for $c/d = 1$. Unlike the variation in $C_y$ for $c/d = 1$, there is no region of flat $C_y$ and $\partial C_y/\partial\alpha$ is positive for all $\alpha$ prior to the sharp change in slope. As $r/d$ is increased to 0.25 for $c/d = 2$, substantially different trends are observed. A much stronger dependence on Reynolds number is observed for this geometry,

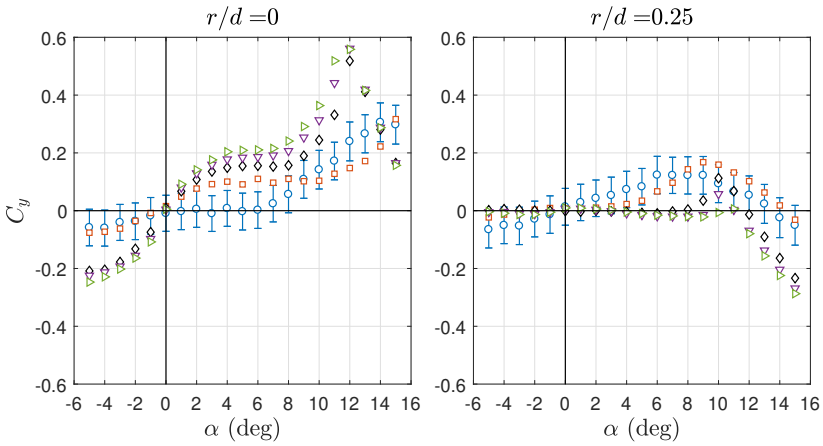


Figure 6: Normal force coefficient variation with $\alpha$ and $Re_d$ for $c/d = 1$. ($\circ$) $Re_d = 1100$, ($\square$) $Re_d = 2500$, ($\diamond$) $Re_d = 5000$, ($\triangledown$) $Re_d = 7500$, ($\triangleright$) $Re_d = 10,000$.



as the slope in $C_y$ at $\alpha = 0°$ is positive for $Re_d = 1100$, but becomes negative at $Re_d = 2500$ and increasingly so with increasing $Re_d$. Interestingly, increasing $r/d$ to 0.25 has a weaker effect on the slope of $C_y$ at $\alpha = 0°$ at $Re_d = 1100$ compared with other Reynolds numbers. The minimum value of $C_y$ for $Re_d > 1100$ increases in magnitude with $Re_d$, along with a slight increase in the $\alpha$ value corresponding to the peak. After this local minimum in $C_y$, each of these cases shows a range of $\alpha$ over which a strong positive gradient in $C_y$ is observed, followed by a smooth transition to a negative gradient at high angle-of-attack. Similar to $r/d = 0$, at high angle-of-attack the effect of Reynolds number decreases and $C_y$ begins to decrease at a comparable rate for all $Re_d$. The behavior of $C_y$ at $r/d = 0.5$ is qualitatively similar to that of $r/d = 0.25$. The most notable difference at this maximum value of $r/d$ is that the slope in $C_y$ at $\alpha = 0°$ varies from flat at $Re_d = 1100$, to slightly positive at $Re_d = 2500$, to negative for all higher $Re_d$. For $Re_d \geq 7500$, the minimum value of $C_y$ is very close to that at $r/d = 0.25$, and it also occurs at $\alpha = 2°$. Once again, a consistent trend that is observed is that Reynolds number effects weaken at high $\alpha$, where in this case $C_y$ data almost collapse for all $Re_d$.

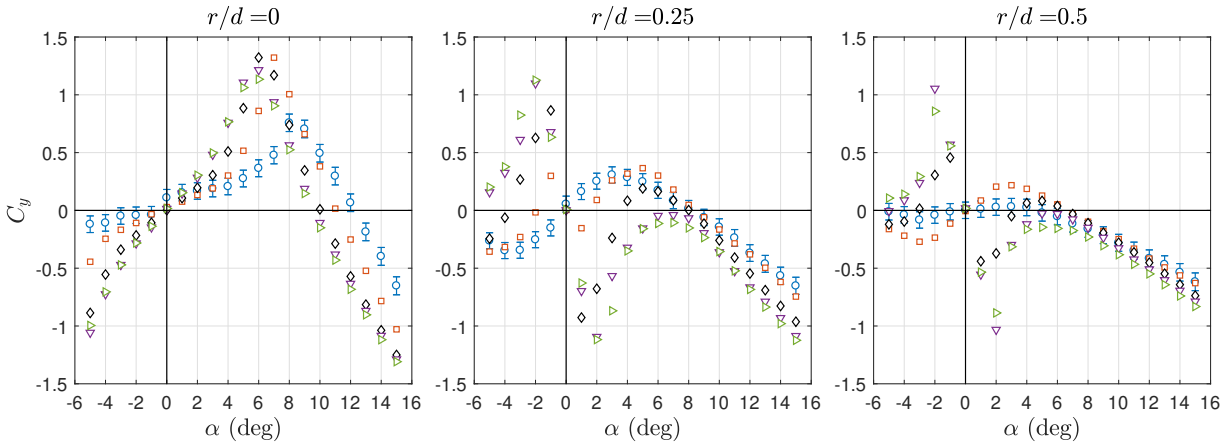


Figure 7: Normal force coefficient variation with $\alpha$ and $Re_d$ for $c/d = 2$. Symbols are the same as in Figure 6.

The remaining plots of $C_y$ for the largest side ratio under investigation, $c/d = 3$, are shown in Figure 8. The results for $c/d = 3$, $r/d = 0$ bear resemblance to those of $c/d = 2$, $r/d > 0$, where $\partial C_y/\partial\alpha$ at

$\alpha = 0°$ shows a strong dependance on Reynolds number. For this geometry, the slope of $C_y$ near zero angle-of-attack is positive and the body is unstable for $Re_d \leq 2500$, but becomes negative and stable for larger Reynolds number. A smooth transition from positive to negative $C_y$ slope with increasing $\alpha$ is observed for $Re_d = 1100$, whereas a sharp transition occurs for $Re_d = 2500$. Unlike $c/d = 2$ and $r/d > 0$, for $Re_d > 2500$ $C_y$ is negative for all positive $\alpha$, and only a small $\alpha$ range can be seen where $C_y$ increases at at relatively low rate. The effect of Reynolds number on $C_y$ undergoes a change once the corner radius is increased above $r/d = 0$, where for both $r/d = 0.25$ and 0.5 the slope of $C_y$ near $\alpha = 0°$ becomes exclusively positive for all $Re_d$. In addition to this, the peak values of $C_y$ show a significant increase compared to $r/d = 0$, with values of $C_y$ reaching as large as nearly 3 in some cases. In fact, the general shape of $C_y$ (which is approximately equal to $-C_L$ for small $\alpha$) for $c/d = 3$ and $r/d \geq 0.25$ is much more reminiscent of that of a streamlined body than that of the other bluff bodies in this study. That is; $C_y$ decreases approximately linearly near $\alpha = 0°$ and $C_y < 0$ for $\alpha > 0$, with only a moderate increase in $C_y$ following the peak minimum before decreasing once again. An interesting double peak behavior is observed for $r/d = 0.5$ and $Re_d \geq 7500$ that is not seen for any other cases. This side ratio also demonstrates consistent behavior where the slope in $C_y$ becomes relatively insensitive to Reynolds number at high angle-of-attack.

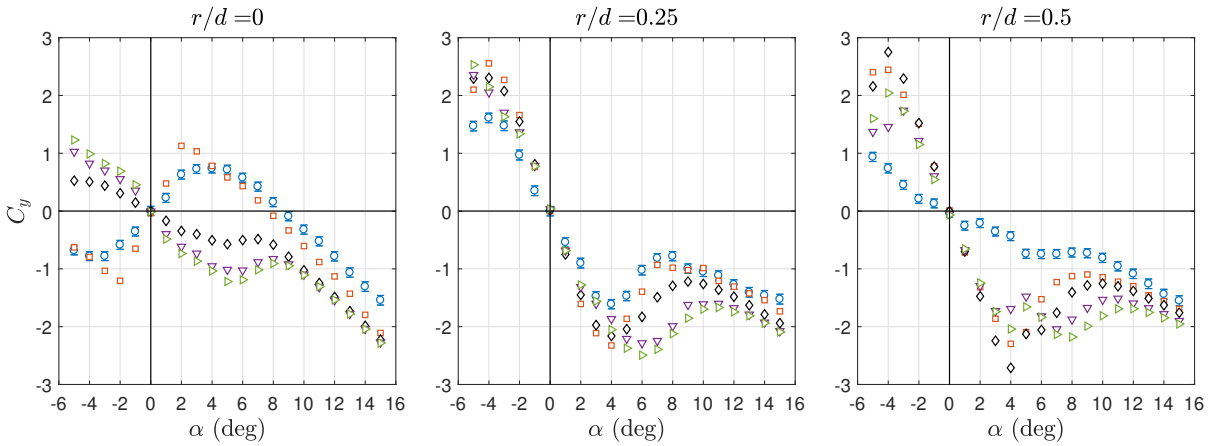


Figure 8: Normal force coefficient variation with $\alpha$ and $Re_d$ for $c/d = 3$. Symbols are the same as in Figure 6.

The effects of $c/d$ and $r/d$ on the galloping criterion, $\partial C_y/\partial\alpha|_{\alpha=0}$, over the Reynolds number range are highlighted in Figures 9 and 10, respectively. Considering first the effects of $c/d$ on galloping, Figure 9 shows that for $r/d = 0$, $\partial C_y/\partial\alpha|_{\alpha=0}$ shows a very similar trend of increasing with Reynolds number for both $c/d = 1$ and 2. In fact, over much of the $Re_d$ range, the values of $\partial C_y/\partial\alpha|_{\alpha=0}$ are within uncertainty of each other for these two side ratios. Once $c/d$ increases to 3, the galloping behavior changes substantially as there is a transition from instability to stability between $Re_d = 2500$ and 5000. For $Re_d < 5000$ where $\partial C_y/\partial\alpha|_{\alpha=0} > 0$, the derivative is an order of magnitude larger for $c/d = 3$, and this body is thus substantially more unstable than $c/d = 1$ and 2. At $r/d = 0.25$, there is no longer similar behavior between $c/d = 1$ and 2, as $c/d = 1$ is neutrally stable for all $Re_d$, whereas $c/d = 2$ transitions from unstable to stable between $Re_d = 1100$ and 2500. A similar transitionary behavior for $c/d = 2$ occurs for $r/d = 0.5$, although in this case at a larger Reynolds number. Once $c/d$ is increased to 3 for both $r/d = 0.25$ and 0.5, these geometries become stable over the entire Reynolds number range. A similarity that can be observed for both $r/d = 0.25$ and 0.5 is that the $\partial C_y/\partial\alpha|_{\alpha=0}$ curves for $c/d = 2$ and 3 appear to converge as $Re_d$ approaches 10,000.

The effects of $r/d$ on the galloping criterion are shown in Figure 10. An overarching observation that can be made for all side ratios is that increasing the corner radius has a stabilizing effect. That is, increasing $r/d$ from 0 to 0.5 can cause the cylinder to transition from unstable to stable at a given Reynolds number. For example, $c/d = 1$ shows this trend at $Re_d = 10,000$. However, for $c/d = 1$ and 2 this stabilizing behavior has a diminishing effect with decreasing Reynolds number, where the value of $\partial C_y/\partial\alpha|_{\alpha=0}$ tends towards 0 for most $r/d$ values. The opposite behavior occurs at $c/d = 3$ where the stabilizing effect of $r/d$ is most pronounced for $Re_d < 5000$, while the effect of $r/d$ becomes negligible at the high Reynolds number end.

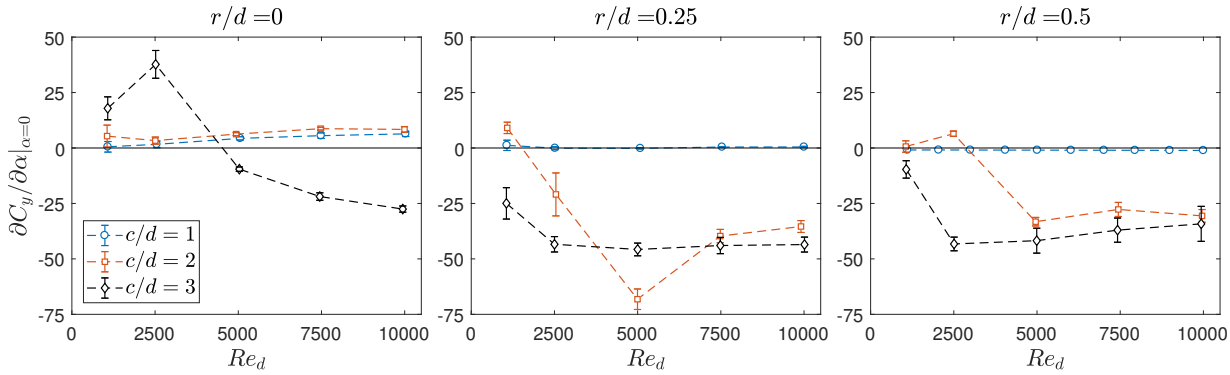


Figure 9: Side ratio effect on the galloping criterion at $\alpha = 0°$ as a function of Reynolds number.

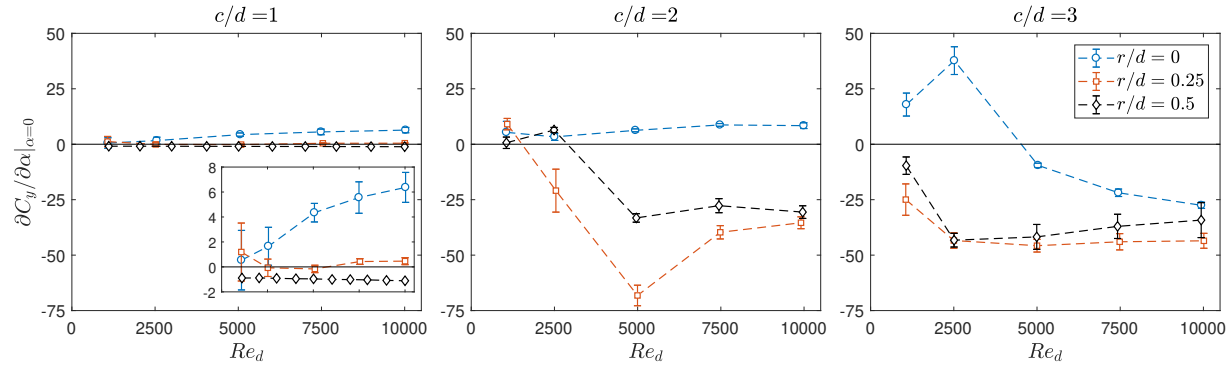


Figure 10: Corner radius effect on the galloping criterion at $\alpha = 0°$ as a function of Reynolds number. The inset plot for $c/d = 1$ has a reduced ordinate scale to highlight the $r/d$ effects.



### C. Surface pressure distributions

Further insight into the effects of cylinder geometry on the flow can be gained by considering surface pressure distributions for select cases. Figures 11 and 12 show the variation in $C_p = (p - p_\infty)/q_\infty$ over the surface, where $p$ and $p_\infty$ are the surface and freestream static pressure, respectively. The pressure coefficient is plotted against the wall-tangential coordinate $s$ normalized by the perimeter, $P$. The cases selected for examining $C_p$ are $c/d = 1$, $r/d = 0$ and 0.25 (Figure 11), and $c/d = 3$, $r/d = 0$ (Figure 12).

Surface pressure distributions at several angles-of-attack and $Re_d = 5000$ for $c/d = 1$, $r/d = 0$ are shown in Figure 11a. In this plot, the dashed vertical lines identify the locations of the corners. As per the definition in Figure 1, $s = 0$ originates at the center of the front face and increasing $s$ travels along the cylinder surface in the clockwise direction. At $\alpha = 0°$, the $C_p$ distribution shows that other than the front face, the flow is separated over the remaining three faces, as indicated by an approximately constant $C_p$ on each of these faces. Once $\alpha$ increases to 4°, the flow remains separated on these faces, however the pressure increases on the upper face ($0.13 \leq s/P \leq 0.38$) but is relatively unchanged on the lower face ($-0.38 \leq s/P \leq -0.13$). This change in the pressure level of the separated flow between the upper and lower faces as $\alpha$ increases from 0° to 4° leads to an increase in $C_y$ and thus instability with respect to galloping, as shown in Figure 5a. As $\alpha$ increases further to 8°, the flow remains separated and the pressure level decreases by a similar amount on both the upper and lower faces, leading to approximately no change in $C_y$. The local maximum in $C_y$ at $\alpha = 12°$ coincides with the flow on the bottom face reattaching near the corner at $s/P = -0.38$, as was expected from previous discussion. Flow reattachment on the bottom face is indicated by the region of substantial pressure recovery that follows the region of separated flow after the $s/P = -0.13$ corner. The flow then separates again from the rear corner over the back face. Similar results are presented for

comparison in Figure 11b for the $c/d = 1$, $r/d = 0.25$ cylinder. For this geometry, the curved faces at the corners are indicated by shaded regions on the plot. The flow at $\alpha = 0°$ is attached over the front corners ($0.07 \leq |s/P| \leq 0.18$) and separates immediately following this. Compared with $r/d = 0$, the value that $C_p$ plateaus to near the rear of the cylinder is substantially larger, which is consistent with lower drag for $r/d = 0.25$. As $\alpha$ increases to 5°, there is a uniform increase in the $C_p$ level over the regions past the top/bottom corners: $-0.5 \leq s/P \leq -0.18$ and $0.18 \leq s/P \leq 0.5$. Unlike $r/d = 0$ where the small $\alpha$ increase leads to relatively little change in $C_p$ on the front face, there are substantial changes in $C_p$ over the front face and front corners for $r/d = 0.25$. However, the pressure decreases over the upper corner and similarly increases over the lower corner, and the sum of all these changes is no change in $C_y$ relative to $\alpha = 0°$ (Figure 6). A substantial change occurs at $\alpha = 10°$ where the pressure minimum decreases at $s/P = -0.18$ and the flow appears to remain attached over a greater extent of the cylinder's lower half, separating near the beginning of the lower back corner ($s/P = -0.32$). This coincides with the local maximum in $C_y$. At $\alpha = 15°$ the behavior remains similar with separated flow after the first corner on the upper half of the model, and attached flow on the bottom half up to the rear corner, which coincides with $C_y$ decreasing and the body becoming stable.



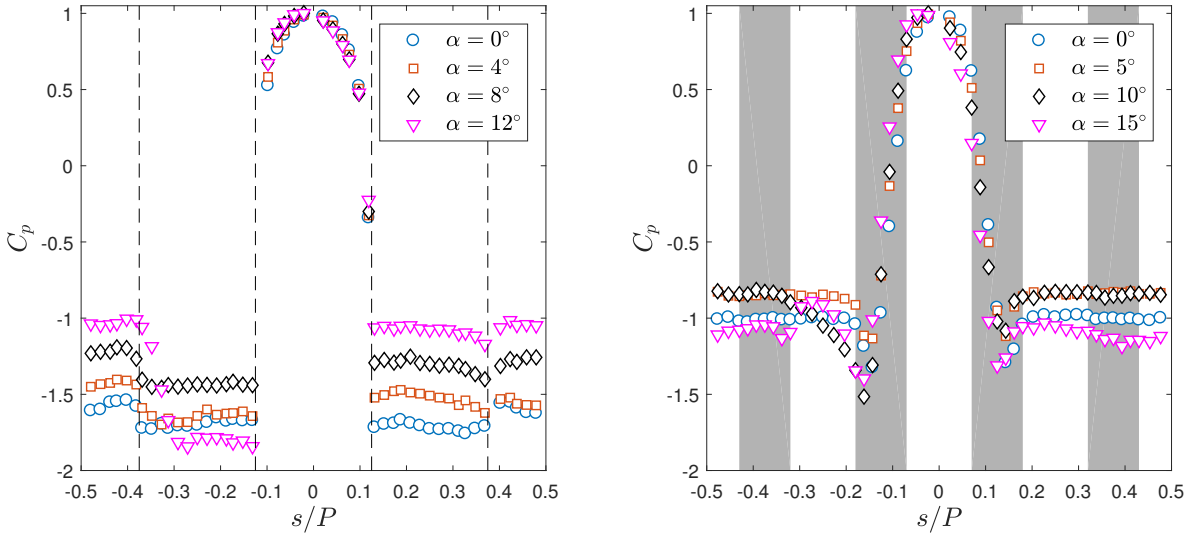


(a) $r/d = 0$. Dashed vertical lines indicate the corners.

(b) $r/d = 0.25$. Shaded areas indicate the curved corner faces.

Figure 11: Surface pressure distributions at various angles-of-attack for $c/d = 1$ and $Re_d = 5000$.

The effect of increasing $c/d$ to 3 for $r/d = 0$ is shown in Figure 12. The flow over the $c/d = 3$ cylinder differs from $c/d = 1$ in that after separation occurs at the front corners ($|s/P| = 0.06$), the flow reattaches at some point near the back corner ($|s/P| = 0.44$) on the top and bottom faces for $\alpha = 0°$. As $\alpha$ is increased to 5°, the flow becomes fully separated on the upper face but on the bottom face the region of separated flow shrinks in length, as indicated by a shorter extent of $C_p$ that is approximately constant. In addition to this, the rate of pressure recovery increases and a local maximum appears in the $C_p$ distribution on the bottom face. Thus, unlike $c/d = 1$ where a small increase in $\alpha$ from $\alpha = 0°$ causes the flow to remain separated on the top and bottom faces and an increase in $C_y$, a shrinking of the separated region for $c/d = 3$ is responsible for the decrease in $C_y$ (Figure 8) and stability with respect to galloping. At $\alpha = 8°$, $C_y$ increases slightly relative to $\alpha = 5°$ and similarly there appears to be very little change in the length of the separated region on the bottom face, although the pressure recovery rate does increase. The separated region shrinks in size as $\alpha$ increases to 15° and there is a substantial increase in the pressure level where $C_p$ is constant, leading to a large decrease in $C_y$. This overall behavior is also consistent at $Re_d = 10,000$ where the shape of $C_y$ is similar. These results suggest the manner in which increasing $c/d$ can lead to galloping stability for $r/d = 0$ at certain Reynolds number is related to whether the flow is able to reattach on the bottom face at

angles-of-attack near zero.

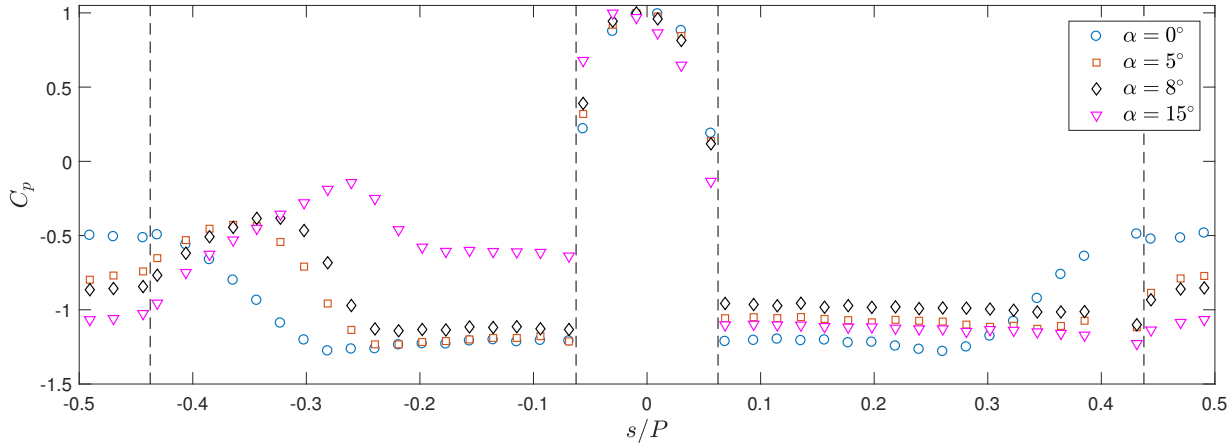


Figure 12: Surface pressure distributions at various angles-of-attack for $c/d = 3$, $r/d = 0$ for $Re_d = 5000$. Dashed vertical lines indicate the corners.

### D. Hard galloping

As shown in Section B, there are certain geometries that are stable with respect to galloping at $\alpha = 0°$ (*i.e.*, $\partial C_y/\partial\alpha|_{\alpha=0} < 0$) but still exhibit ranges of $\alpha$ where $\partial C_y/\partial\alpha > 0$, thereby making them susceptible to hard galloping. This feature is observed for $c/d = 2$ and 3, with dependence on $Re_d$ and $r/d$. The behavior of $\partial C_y/\partial\alpha$ over $0 \leq \alpha \leq 15°$ is shown in Figure 13 for four cases with two side ratios and two corner radii: $c/d = 2$ and 3, and $r/d = 0.25$ and 0.5. The results demonstrate for each of these four geometries, there are one to two ranges of $\alpha$ where $\partial C_y/\partial\alpha > 0$ and the body could exhibit hard galloping. At $Re_d = 5000$, the $c/d = 2$, $r/d = 0.25$ geometry shows a transition to $\partial C_y/\partial\alpha > 0$ at approximately 1°, and this angle will be referred to as the galloping angle. When $c/d$ is increased to 3 for the same corner radius, the galloping angle increases to $\sim 4°$. Interestingly, the geometries with $r/d = 0.5$ show the same galloping angle as that for $r/d = 0.25$ at the same $c/d$. The angle at which $\partial C_y/\partial\alpha$ transitions back to negative also remains relatively unchanged with $r/d$. The main difference observed is that for $c/d = 3$, $r/d = 0.5$ there are two closely spaced regions of $\partial C_y/\partial\alpha > 0$. This hard galloping behavior is consistent at $Re_d = 10,000$ for $c/d = 2$, although for $c/d = 3$ the galloping angle is reduced for $r/d = 0.5$ compared with 0.25. These results demonstrate that for $Re_d$ and $r/d$ cases where hard galloping is observed, the galloping angle is mainly governed by $c/d$. This is in exception to $c/d = 3$ at $Re_d = 10,000$. The galloping angle is related to the susceptibility to hard galloping, since a larger galloping angle is equivalent to a larger initial disturbance that would be required for an elastically mounted body to reach that value of $\alpha$ instantaneously. Since the galloping angle tends to increase with side ratio, this leads to a decrease in the susceptibility to hard galloping.

## IV. Conclusions

This experimental study investigates the effects of side ratio and corner radius on the galloping behavior of rectangular cylinders at Reynolds numbers between 1000 and 10,000. Three different $c/d$ values are considered, 1, 2, and 3, along with three different corner radii: $r/d = 0$, 0.25 and 0.5. Lift and drag forces are measured for varying angles-of-attack and Reynolds number, and from this the normal force coefficient is computed. The variation in $C_y$ (the force coefficient in the galloping direction) with angle-of-attack is used to asses the galloping behavior of each geometry. In addition to this, surface pressure distributions are presented for $c/d = 1$, $r/d = 0$ and 0.25, and $c/d = 3$, $r/d = 0$.

The effect of $c/d$ on the galloping criterion, $\partial C_y/\partial\alpha|_{\alpha=0}$, varies for different $r/d$. At $r/d = 0$, $c/d = 1$ and 2 are unstable and had similar values of $\partial C_y/\partial\alpha|_{\alpha=0}$ over the entire Reynolds number range. This behavior changes drastically when $c/d$ is increased to 3, and the body shows a transition from unstable to

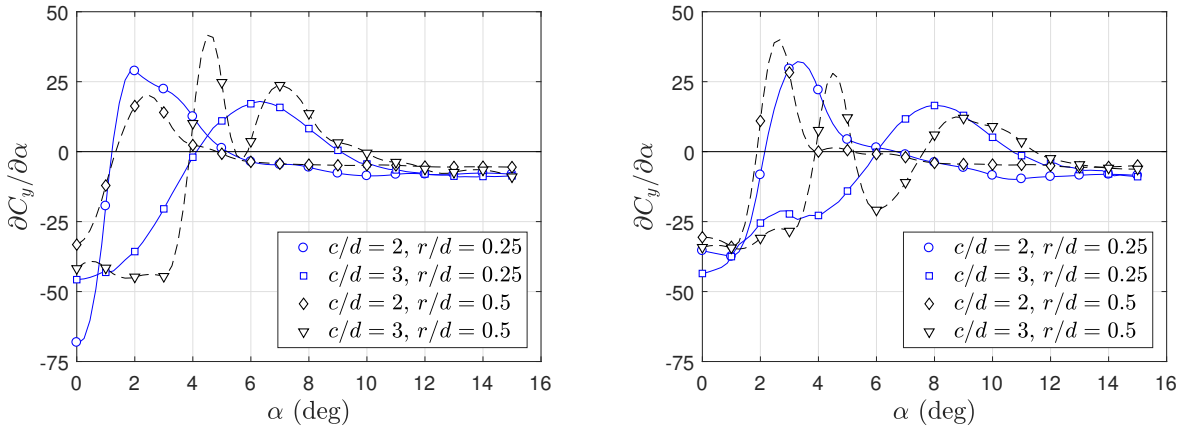


(a) $Re_d = 5000$ (b) $Re_d = 10,000$

Figure 13: Galloping criterion versus angles-of-attack for $c/d = 2$ and 3, $r/d = 0.25$ and 0.5 at $Re_d = 5000$ and 10,000. Solid lines indicate $r/d = 0.25$, dashed lines indicate $r/d = 0.5$.



stable behavior as the Reynolds number increases above 2500. A unique case is $c/d = 1$, $r/d = 0.25$ where $\partial C_y/\partial\alpha|_{\alpha=0} \approx 0$ for all $Re_d$ and the body is therefore neutrally stable. For the same $r/d$, $c/d = 2$ shows a transition from unstable to stable conditions with increasing $Re_d$, while $c/d = 3$ is stable over the entire $Re_d$ range. This behavior for $c/d = 2$ and 3 remains the same at the largest $r/d$ of 0.5.

In general, increasing $r/d$ above 0 is found to have a stabilizing effect on the body. This is most noticeable at the high end of the Reynolds number range for $c/d = 1$ where the behavior transitions from unstable, to neutrally stable, to stable for $r/d = 0$, 0.25 and 0.5, respectively. For $c/d = 2$ and similar Reynolds numbers, the effect of $r/d$ is more dramatic as the increase from $r/d = 0$ to 0.25 is sufficient for stability. This stabilizing effect diminishes with decreasing $Re_d$ for $c/d = 1$ and 2, where in each case $\partial C_y/\partial\alpha|_{\alpha=0}$ approaches zero for all $r/d$ with decreasing $Re_d$ (other than the circular cylinder). This trend reverses for $c/d = 3$, where the low Reynolds number range shows the most sensitivity to $r/d$ and at the high Reynolds number end $c/d = 3$ is stable irregardless of $r/d$.

Surface pressure distributions are used to gain insight into the nature of the flow as it relates to galloping stability. For $c/d = 1$, $r/d = 0$, which is unstable, the increase in $C_y$ with increasing $\alpha$ near $\alpha = 0°$ is related to the flow on the upper and lower faces of the cylinder remaining separated. Once the flow reattaches on the bottom face, a maximum in $C_y$ occurs and the slope with $\alpha$ becomes negative. This is similarly observed for $c/d = 1$, $r/d = 0.25$ where the formation of a larger region of attached flow on the bottom half of the cylinder coincides with a maximum in $C_y$. Unlike $c/d = 1$, the flow on the upper and lower surfaces for $c/d = 3$, $r/d = 0$ separates but reattaches at $\alpha = 0°$. A small increase in $\alpha$ causes a shrinking of the length of the separated domain, and thus a decrease $C_y$ and a body that is stable with respect to galloping.

The final aspect of this study concerns the susceptibility of geometries that are stable to becoming unstable as hard oscillators, known as hard galloping. This effect is observed for $c/d = 2$ and 3, in particular for $r/d = 0.25$ and 0.5. The results demonstrate that side ratio has a dominating effect on hard galloping, as the galloping angle for a particular $c/d$ is generally unchanged with $r/d$. Increasing the side ratio from 2 to 3 increases the galloping angle, and thus makes the body less susceptible to hard galloping.

## Acknowledgments

This project is funded through ARO grant number W911NF1710153. The views and conclusions contained in this document are those of the authors and should not be interpreted as representing the official policies, either expressed or implied, of ARO or the U.S. Government. The U.S. Government is authorized to reproduce and distribute reprints for Government purposes notwithstanding any copyright notation herein.

## References


[1] Blevins, R. D., *Flow-induced vibration*, Krieger Publishing Company, 2nd ed., 2001.

[2] Siefers, T., Greene, K., McLaughlin, T., and Bergeron, K., "Wind and water tunnel measurements of parachute suspension line," *51st AIAA Aerospace Sciences Meeting including the New Horizons Forum and Aerospace Exposition*, No. 2013-0064, 2013.

[3] Bergeron, K., Ecklebe, D., McClure, K., Johari, H., Curlett, T., and Pitman, B., "Parachute suspension line drag analysis," *20th AIAA Aerodynamic Decelerator Systems Technology Conference and Seminar*, No. 2009-2982, 2009.

[4] Bearman, P. and Luo, S., "Investigation of the aerodynamic instability of a square-section cylinder by forced oscillation," *Journal of Fluids and Structures*, Vol. 2, No. 2, 1988, pp. 161–176.

[5] Siefers, T. M., McLaughlin, T. E., and Bergeron, K., "Wind tunnel characterization of fluid-structure interactions for various suspension lines," *44th AIAA Fluid Dynamics Conference*, No. 2014-2771, 2014.

[6] Noda, H. and Nakayama, A., "Free-stream turbulence effects on the instantaneous pressure and forces on cylinders of rectangular cross section," *Experiments in fluids*, Vol. 34, No. 3, 2003, pp. 332–344.

[7] Huang, R., Lin, B., and Yen, S., "Time-averaged topological flow patterns and their influence on vortex shedding of a square cylinder in crossflow at incidence," *Journal of Fluids and Structures*, Vol. 26, No. 3, 2010, pp. 406–429.

[8] Carassale, L., Freda, A., and Marrè-Brunenghi, M., "Experimental investigation on the aerodynamic behavior of square cylinders with rounded corners," *Journal of fluids and structures*, Vol. 44, 2014, pp. 195–204.

[9] Luo, S., Yazdani, M. G., Chew, Y., and Lee, T., "Effects of incidence and afterbody shape on flow past bluff cylinders," *Journal of Wind Engineering and Industrial Aerodynamics*, Vol. 53, No. 3, 1994, pp. 375–399.

[10] Norberg, C., "Flow around rectangular cylinders: pressure forces and wake frequencies," *Journal of wind engineering and industrial aerodynamics*, Vol. 49, No. 1-3, 1993, pp. 187–196.

[11] Piccardo, G., Carassale, L., and Freda, A., "Critical conditions of galloping for inclined square cylinders," *Journal of Wind Engineering and Industrial Aerodynamics*, Vol. 99, No. 6-7, 2011, pp. 748–756.

[12] Parkinson, G. and Smith, J., "The square prism as an aeroelastic non-linear oscillator," *The Quarterly Journal of Mechanics and Applied Mathematics*, Vol. 17, No. 2, 1964, pp. 225–239.

[13] Parkinson, G. and Brooks, N., "On the aeroelastic instability of bluff cylinders," *Journal of applied mechanics*, Vol. 28, No. 2, 1961, pp. 252–258.